Planar Aerial Reorientation of an Insect Scale Robot Using Piezo-Actuated Tail Like Appendage

Avinash Singh

A thesis submitted in fulfillment
of the requirements for the degree of

Master of Science in Mechanical Engineering

University of Washington

2018

Committee:

Sawyer B. Fuller, Chair

Ashis Banerjee

Samuel Burden

Thomas Daniel

Program Authorized to Offer Degree:
Mechanical Engineering

University of Washington

Abstract

Planar Aerial Reorientation of an Insect Scale Robot Using Piezo-Actuated Tail Like Appendage

Avinash Singh

Chair of the Supervisory Committee:
Professor Sawyer B. Fuller
Department of Mechanical Engineering

Robots today, though capable of performing a growing number of increasingly complex tasks, lack the agility that would be required to perform in a rapidly changing or dynamic environment, especially when compared to animals and insects, they are very rigid in performance. Recent developments in the field of insect-scale flapping wing micro-robots include controlled hovering flight, sensor integration and controlled landing. However, their ability to perform rapid, dynamic motions has not been explored in depth.

We present the design, fabrication, and actuation of a insect-sized (142 mg) aerial robot that is equipped with a bio-inspired tail. Incorporating a tail allows the robot to perform rapid inertial reorientation as well as to shift weight to actuate torques on its body. Here we present the first analysis of tail actuation using a piezo actuator, departing from previous work to date that has focused exclusively on actuation by DC motor. The primary difference is that unlike a geared motor system, the piezoelectric-tail system operates as a resonant system, exhibiting slowly-decaying oscillations. We present a dynamic model of piezo-driven inertial reorientation, along with an open-loop feedforward controller that reduces excitation of the resonant mode. Our results indicate that incorporating a tail can allow for more rapid dynamic maneuvers and could stabilize the robot during flight.

TABLE OF CONTENTS

LIST OF FIGURES

ACKNOWLEDGMENTS

First and foremost, I would like to thank my advisor and mentor, Dr. Sawyer Fuller for his encouragement and support for this research. He helped me come up with the thesis topic, encouraged creativity in every aspect of this work and guided me over almost a year and a half of development.

A sincere thanks to my co-mentor Dr. Thomas Libby. This work would not have been in its current shape without his participation, constant inputs and precise nudges in the right direction.

I would like to thank my thesis committee, Dr. Ashis Banerjee, Dr. Samuel Burden and Dr. Thomas Daniel for their insightful comments and the hard questions.

I would also like to thank all my fellow lab-mates at the Autonomous Insect Robotics Lab for all their help, s timulating conversations and nerdy pun-loaded jokes. This work was made more fun by the counsel of my friends. Their patience and encouragement play a big part in the culmination of this work.

I am forever grateful to my parents, Dr. Tarkeshwar and Dr. Asha, and my brother, Rohit, for their spiritual support and wise counsel.

Last but not least, to caffeine and to second chances.

DEDICATION

To my parents

Chapter 1

MOTIVATION AND PREVIOUS WORK

The motivation to create small agile, maneuverable and capable robots approximately the size of a honeybee (∼100 mg) is driven by the engineering challenges associated with miniaturization and their potential for improved performance on robotic tasks. Significant advancements have been made in several areas including the development of new laser-based fabrication technology suitable for building insect-scale articulated mechanisms and actuators [1, 2, 3, 4]. These have been used to realize advancements in insect-scale flight capabilities including the first liftoff [5], passively-stabilized attitude [6], hovering and controlled flights [7], and landing [8]. Sensor integration aimed at achieving autonomy has included on-board vision [9, 10], gyroscopic stabilization [11], using wind sensing antennae to sense air speed [12] and pitch and yaw control with on-board magnetometer [13]. Unsteady maneuvers such as perching on a horizontal surface [14], perching on a vertical surface [15], and wind disturbance rejection [16] have also been demonstrated.

The aforementioned work has demonstrated that insect-sized robots are capable of rapid, dynamic maneuvers, particularly [15], which demonstrated angular accelerations nearly 20,000 deg/s^2. This compares favorably with the 10,000 deg/s^2 that was achieved by a larger, 0.5 kg quadrotor-style helicopter, the Ascending Technologies X-3D performing flips [17]. However, it is often desirable to have even greater maneuvering capabilities. In this paper, we consider one possible path to increased agility - an actuated, weighted appendage for Inertial Reorientation (IR) [18]. IR, defined as control of body orientation through inertial forces that arise from internal configuration changes, has been deployed on robots from a few grams to over 10 kg. A common adaptation that provides additional maneuvering capability in nature is an actuated appendage with sufficient mass to reorient the body when it is moved. This type

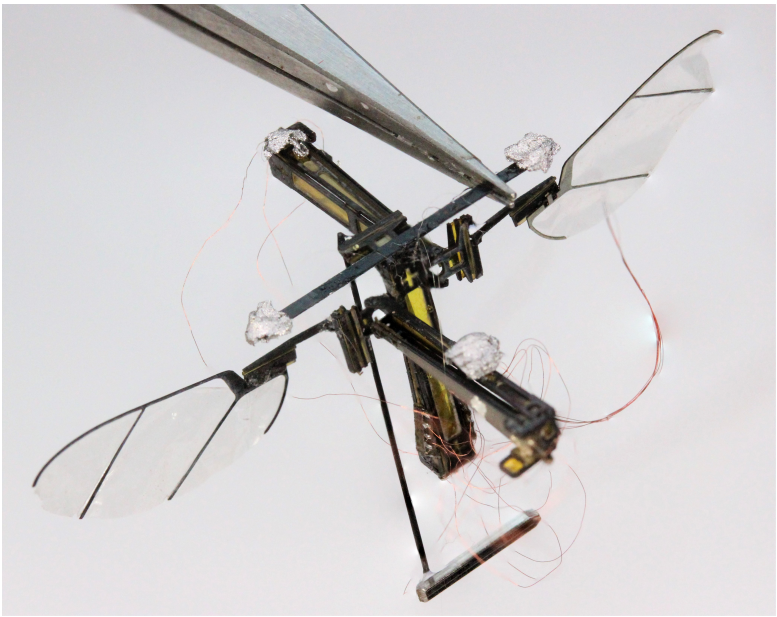

Figure 1.1: Honeybee-sized aerial robot equipped with a piezo-actuated tail (at bottom).

of actuation is known as Inertial Reorientation (IR), and it involves a net zero angular momentum rotation of both the body and appendage, in opposite directions [19, 20]. Examples include abdominal movements in the hawkmoth to control flight motions a variety of animal morphologies including lizards [21, 22], and moths [23, 24]. The addition to an appendage, to which we will refer subsequently as a tail, can facilitate both rapid rotation maneuvers as well as more precise small rotational maneuvers. Both of these are useful in the context of control, allowing for rapid midair maneuvers such as rapid turns, or careful reorientation prior to landing to optimize landing gear placement. Recent developments include robots performing feats like aerial reorientation [19], precise and rapid yaw changes [25], rapid turns [26, 27], dynamic self righting [28], disturbance rejection [29, 30], pitch control in mid air during a jump [31]. Inertial appendages have also been applied in thrust redirection [32].

Here, we explore inertial reorientation on an insect-sized robot. In previous robot work, the appendage was actuated by a DC electric motor. As scale reduces to that of a honeybee-sized insect, however, these motors become inefficient and have a low power density [33]

because of unfavorable scaling physics [34]. Here, we use the same actuator that has previously used successfully to actuate the wings of insect-sized robots: a piezoelectric bimorph cantilever actuator. As in the wing-actuation system, this actuator is combined with a specially designed transmission, emulating a four-bar kinematic chain [35] to magnify actuator displacement. The transmission amplifies a $\sim$500 μm tip motion into 70°–120° angular movement of the wing or tail. As with the actuator-wing system, the actuator-tail system is a resonant system. This characteristic is used productively in the wing system to amplify wing motion near the resonant frequency of the flapping wings, which is around 150 Hz. However, when actuating a tail, the same resonance results in undesirable oscillations with a long decay time. As part of our work we propose a solution that includes a means to construct a dynamic model that permits feedforward cancellations of these oscillations. To our knowledge this work represents the first piezo-actuated tail reorientation system, and the first insect-sized robot to be equipped with a tail.

The outline of this thesis is: Chapter. 2 describes introduces models of the robot and its actuator, chapter. 3 describes the robot design, chapter. 4 describes how the robot was fabricated, chapter. 5 describes the design of the feedforward controller applied in this work, chapter. 6 provides the results including open loop experiments, and conclusions and future work in chapter. 7.

Chapter 2

MODELING AND ANALYSIS

Previous work on aerial inertial reorientation analyzed a number of candidate morphologies, including tails and flywheels [18]; we will leverage these models to design the robots discussed in this work.

2.1 Actuator Behavior

As it is central to the analysis in this paper, we start with the operation of the piezo actuator. A diagram of how it operates to drive a wing or tail is given in Fig. 2.1. The piezo cantilever consists of a carbon fiber layer sandwiched between top and bottom layers of the piezo ceramic material. The top and bottom surface of each piezo sheet are coated with a thin conductor so that the electric potential is the same across the sheet. To drive the piezoelectric actuator, the top piezo layer is given a constant positive bias voltage (+300V) and the bottom piezoelectric layer is grounded (0V). To drive motion, the middle, carbon fiber layer is given a signal voltage somewhere been these two extremes. As a result of the piezoelectric effect, the piezo material deforms in approximate proportion to the strength of the electric field, resulting in a force at the tip of the cantilever. The cantilever configuration amplifies the small piezoelectric strain, and the transmission amplifies it still further.

A piezoelectric actuator in tandem with a motion-amplifying transmission differs from a DC motor because the cantilevered actuator impart a spring-like stiffness to the system. Additionally, the flexures in the transmission add additional stiffness. Under the three assumptions mentioned in [35], namely, operation of the actuator with an ideal voltage source, operation of the actuator with a frequency much lower than its self-resonant frequency, and assuming negligible aerodynamic drag, the piezoelectric actuator can be assumed to behave

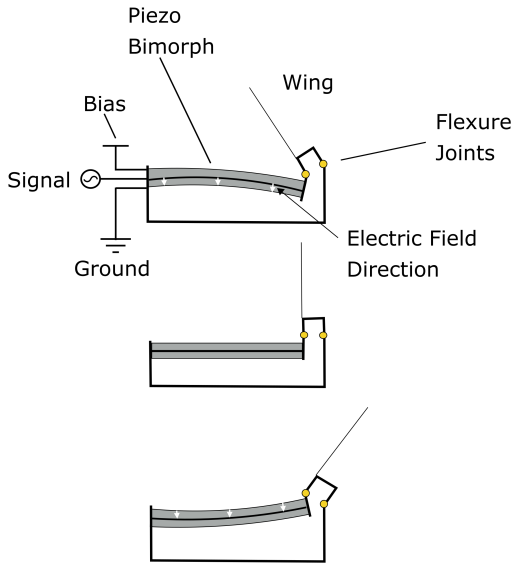

Figure 2.1: Diagram of the mechanism of piezoelectric antilever actuation of the wings. The piezo actuator drives large-amplitude wing motion through small strain changes. The piezo actuator is configured as a bimorph cantilever, consisting of a carbon fiber layer sandwiched between top and bottom piezo sheets. The top surface of the bimorph is charged to a constant high voltage, while the bottom surface is tied to ground per "simultaneous drive" configuration. An alternating signal is connected to the middle layer, providing an alternating electric field in the piezo material. This produces alternating small strains through the reverse piezoelectric effect, which is manifested as motion at the tip of the cantilever. A microfabricated transmission amplifies these tip motions into large ($\sim$ 90 deg) wing motions. This diagram shows the mechanism as seen from above; motion of the wings causes airflow downward, into the page.

linearly. This allows us to additionally assume that there is a linear relation between torque applied and input voltage. For an appendage with angle θ_r, driven by the the piezoelectric

actuator through a linkage, the torque applied to the appendage is:

$$\tau_a = \rho V - K\theta_r \tag{2.1}$$

where K is the resulting rotational spring constant of the actuator-transmission system and ρ is a constant that relates applied voltage V to actuator torque on the tail. We identified both ρ and K empirically, as described in chapter. 6.

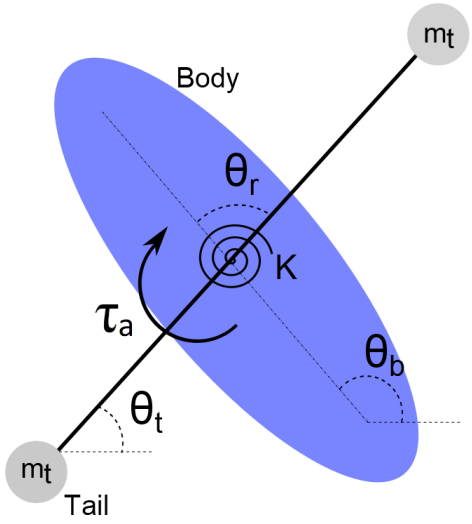

Figure 2.2: Diagram of the reorientation template model of dynamics of our test-bed robot. To make its center of mass coincident with the pivot point, the tail is composed of a massless rigid bar and masses at either end.

2.2 Reductive Modeling

To analyze our system, we make use of the notions of a templates and anchors, concepts taken from biology to help in understanding potentially complicated mechanical systems. Full and Koditschek [36] define a template as a formal reductive model with least number of variables and parameters that exhibits a targeted behavior that suggests their underlying control strategies which is verified by testing against empirical data. Anchors, being more

elaborate models, introduce representations of specific details of interest. Anchors are still reductive models as they too have removed motions and redundancies to produce a less over constrained model to develop detailed control approaches. To provide an example, a template model of human running is a spring-loaded inertial pendulum (SLIP), which consists of only a spring, a mass, and a pendulum body. An anchor consists of the more complicated series of leg joints that produce this behavior. These two representations provide different levels of reductive modeling to help explain the much more complicated behavior of the actual human.

The simplest and most analytically tractable of these models (*Template*) consists of two rigid bodies, with a joint coincident with their centers of mass (CM) as seen in Fig.2.2 . This model was analyzed to provide a concise relationship between body design and performance, but utilized a DC motor-like model to constrain reorientation time. Here, we will redesign the template with a piezo-like motor model, and derive a new controller to achieve reorientation. We will use this model to design two prototypes, one that hews closely to the template for simple analysis, and another with an offset tail that enables better flight performance.

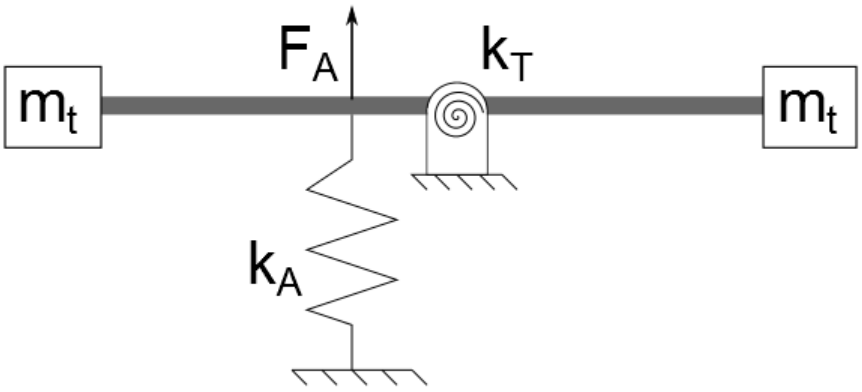

Figure 2.3: Linear dynamic model of the actuator system

2.3 A Piezo-driven Inertial Reorientation Template

This section adapts the Inertial Reorientation (IR) Template [18] to a piezo-like actuator model. Fig. 2.3 shows a linear dynamic model of the actuator and tail, similar to [35] with mass being added at both ends of the tail. F_a is the force at the tip of the actuator, k_A is the actuator stiffness, k_T is the transmission stiffness and m_t being the mass at the tip of the 'tail'. This system is then converted to a rotational system shown in Fig.2.4. The tail moment of inertia (MOI) I_t and body MOI I_b are shown along with the total system stiffness K and torque applied by the piezoelectric actuator τ_a. θ_t and θ_b are the angular displacements of the tail and body respectively.

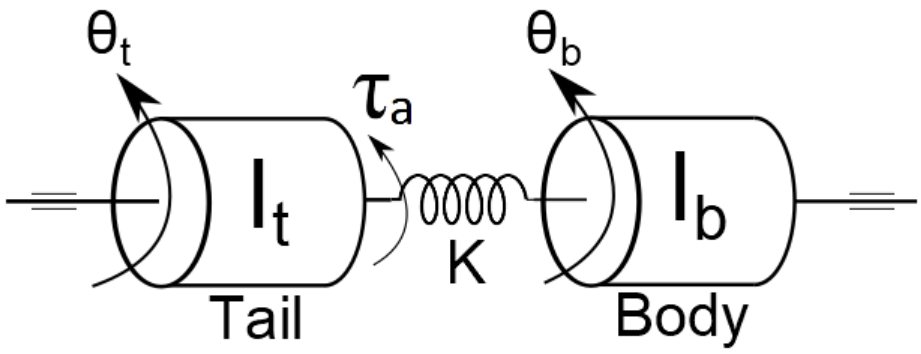

Figure 2.4: Rotational model of the actuator system

The template, shown in Fig.2.2 in this work is defined as a planar system consisting of two bodies, the "body" and the appendage or "tail". The two bodies have a common center of mass which is also the "pivot" modeled as a pin joint.

The actuator applies a torque τ_a on the tail, and an equal and opposite torque on the body (the orientation of which is denoted θ_b). The quantity θ_r is the relative angle between the two bodies. The template is assumed to be falling or floating in space with no external forces, so that angular momentum about the CM is conserved.

Libby *et. al* [18] defined *Inertial Effectiveness* of the IR system as a dimensionless

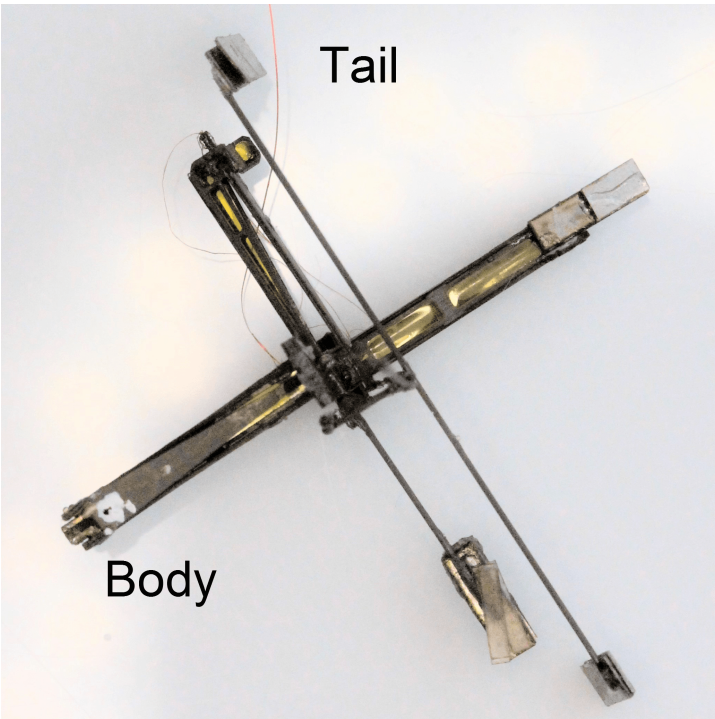

Figure 2.5: Robotic testbed designed to be as close as possible to the ideal template, including an additional mass (lower right) so that its center of mass is coincident with the pivot point of the tail.

constant, ξ, which is the ratio of the tail moment of inertia (MOI) I_t, normalized by the sum of the body MOI (I_b) and the tail MOI,

$$\xi = \frac{I_t}{I_b + I_t} \tag{2.2}$$

This parameter characterizes the ratio of body velocity to relative appendage velocity for the template under zero-angular momentum reorientation. Defining an initial condition, $\theta_b(0) = \theta_r(0) = 0$, ξ kinematically relates the body angle to the relative angle,

$$\theta_b = -\xi\theta_r \tag{2.3}$$

The dynamics of the body follow from Euler's law, $I_b\ddot{\theta} = \tau_a$. Plugging in the actuator

model, Equation. 2.1, the dynamics are,

$$I_b\ddot{\theta}_b = \rho V + K\theta_r \tag{2.4}$$

Since body angle is related to relative angle by (2.3), (2.4) can be rewritten in terms of the body orientation, θ_b only, so that the relative angle θ_r disappears,

$$\ddot{\theta}_b = \frac{\rho V}{I_b} - \frac{K}{\xi I_b}\theta_b. \tag{2.5}$$

In contrast to the DC-motor based IR template, whose dynamics were speed-dependent, the piezo-based IR template takes the form of a forced, undamped harmonic oscillator.

2.4 State Space Model

To simulate the system's response, we developed a state space model for the system in the form $\dot{x} = Ax + Bu$, where states $x = [\theta_b,\ \dot{\theta}_b]^T$, consist of the angular position and angular velocity of the body and the control input $u = \tau_a$, is the torque at the tip of the actuator with matrices A and B as:

$$A = \begin{bmatrix} 1 & 0 \\ \frac{-K}{I_b\xi} & 0 \end{bmatrix} \qquad B = \begin{bmatrix} 0 \\ I_b \end{bmatrix}$$

Chapter 3

ROBOT DESIGN AND DRIVING SETUP

3.1 Morphology Design

In order to study the effects of inertial reorientation of a tail on an existing insect scale robot, we modified a Robofly created by Chukewad *et. al.*. The RoboFly [37] [38] [39] is a 74 mg flapping wing robot, designed and fabricated at the Autonomous Insect Robotics lab at the University of Washington. It is designed to operate through two flapping wings actuated by two independent piezoelectric bi-morph actuators. In its original configuration, one actuator points forward and the other aft, so that the mass is balanced about the wings. For this work, we altered this basic design by adding an additional identical actuator unit between these two, mounted perpendicularly. This third actuator drives the tail (Fig. 1.1). For our simplified device operating with template dynamics, we removed the wings and added a counterbalance (Fig. 2.5).

In our prototype, the range of available stroke angle of the tail was found to be approximately 70°. The stroke is chosen as the max available in each direction to affect maximum reorientation of the body. To design our tail, we aimed to achieve an effectiveness of approximately 50%, so by Equation. 2.3, we could servo the body up to 35°. The tail length l_t was chosen to be 15 mm, long enough to avoid any obstruction to the wire tethers that attach to the actuator at ≈12 mm from the pivot. To estimate the body's inertia I_b, we used approximation of the moment of inertia of a single actuator-airframe taken from a computer model in [3] and multiplied it by four (three actuators and one counterweight). Using this number in the effectiveness equation (Equation (2.2)), we were able compute a desired tail inertia. Assuming the masses at the end of the tail act as point masses, we calculated their

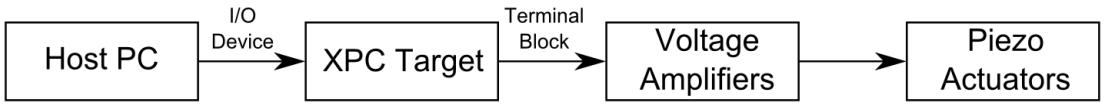

Figure 3.1: Block diagram showing the open loop setup applied to drive the piezoelectric actuators

necessary mass m_t from

$$I_t = 2l_t^2 m_t,$$

neglecting the mass of the connecting carbon fiber rod, which weighed less than 3 mg. Length and mass of the tail can be found in 6.3.

3.2 High-voltage piezo signal

As shown in Fig. 3.1, we used a Simulink Real-Time (formerly xPC Target) (Mathworks, Natick, MA) and a data aquisition board with analog output capability (National Instruments model PCI-6259) to generate analog signals. These were amplified using a piezo amplifier (Trek model 2205).

Simulink model created on a Host PC and XPC target, a host-target prototyping environment, executing the Simulink model in real time. The model parameters are set using MATLAB. The Host-XPC Target communication is established over Ethernet. The outputs of this Simulink real time model are driving voltages sent to I/O boards and then to voltage amplifiers which provide suitable driving voltage to the piezoelectric actuators.

Chapter 4

FABRICATION

The robot was fabricated by laser micromachining using diode-pumped solid-state (DPSS) frequency tripled Nd:Yag laser with 355 nm wavelength (PhotoMachining, Inc.) and pin-aligned multilayer thermal sheet adhesion[1]. Fig. 4.1 shows a close-up of a single actuator unit.

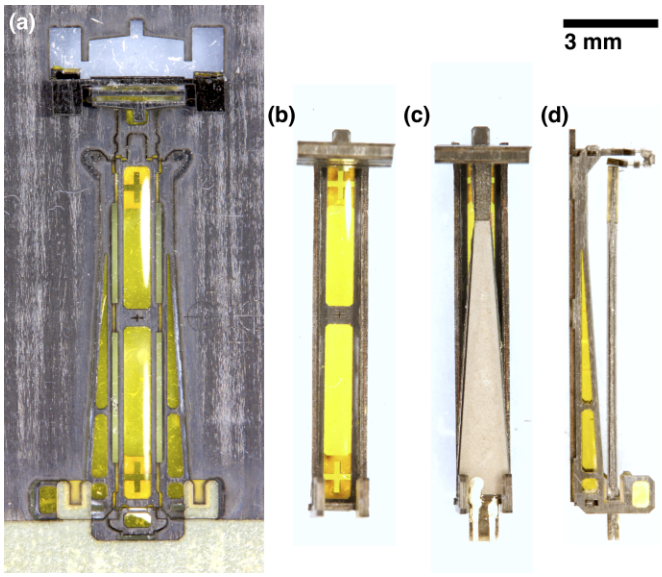

Figure 4.1: Close-up image of the design and folded construction of the actuator-frame unit. (a) The laminate in its scaffolding after the transmission component has been folded downward. (b) The scaffolding is cut from the airframe and folded. (c), (d) Top and side views of the frame after the piezo actuator has been incorporated.

Our design [37], departs from an earlier design [3] by creating the airframe from a single part rather than approximately 9 separate parts, simplifying fabrication. Using a single

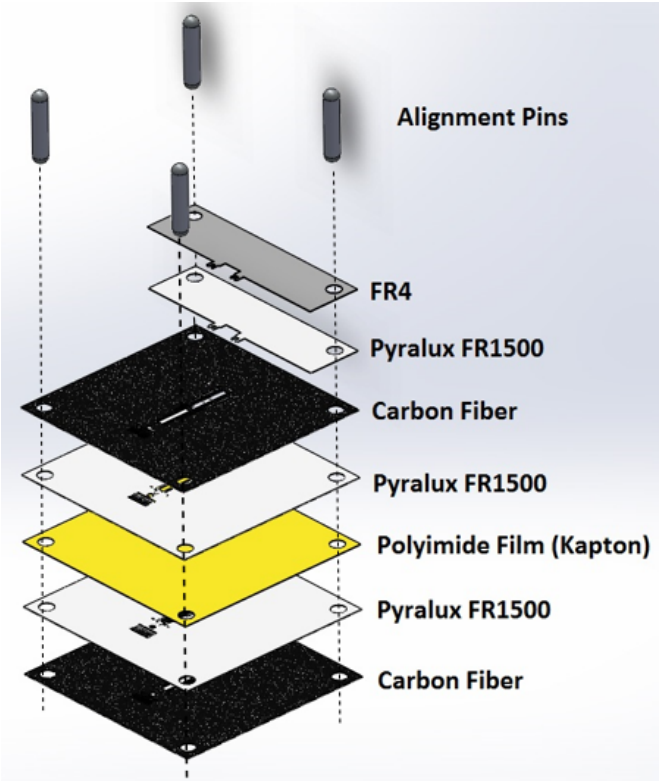

Figure 4.2: Exploded view of the different layers used in fabrication of an airframe before curing

laminate sheet rather than discrete components also allows for features like castellated folds and mechanical locks.

The laminate has uniquely designed castellated joints that depend on mechanical interlocking of the surfaces and confined angular movement due to this interlocking for a precise fit. The folds are designed to have a predefined angles specified by either a stop defined by the mechanical contact with another surface or a stop resulting from castellated folds. The thickness of a castellation is a function of the total laminate thickness so that the laminate has a passive stop at 90°. The laminate is machined and a unit of the robot is assembled using the following general steps:

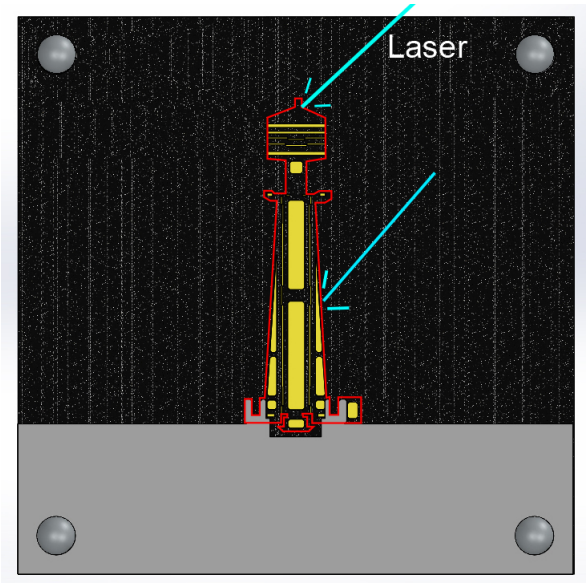

Figure 4.3: Layup after being cured under predetermined pressure and temperature, with initial release cuts being performed

- Laser Machining: A diode-pumped solid-state laser with 355 nm wavelength (PhotoMachining, Inc.) is used to machine two carbon fiber layers, three modified acrylic adhesive (FR1500 Pyralux) layers, one flexible polyimide film (Kapton) and one glass-reinforced epoxy laminate (FR-4) layer. The layers are machined with features which are designed with alignment in mind.The polyimide layer acts as flexure material, providing flexibility and also surface to fold. The pyralux layers are the adhesive layers. FR-4 is used to insulate the actuator surface from the carbon fiber bodies, thus preventing shorts when high driving voltages are implied.

- Layup Creation: An alignment block and polished stainless steel pins are used to manually align these layers and ensure that the features are placed correctly. This layup is shown in Fig.4.2.

- Curing: The layup is then cured in a heat press at predetermined temperature (200°C)

and pressure (50 kg). The temperature ramp rate is 1000°C/min)

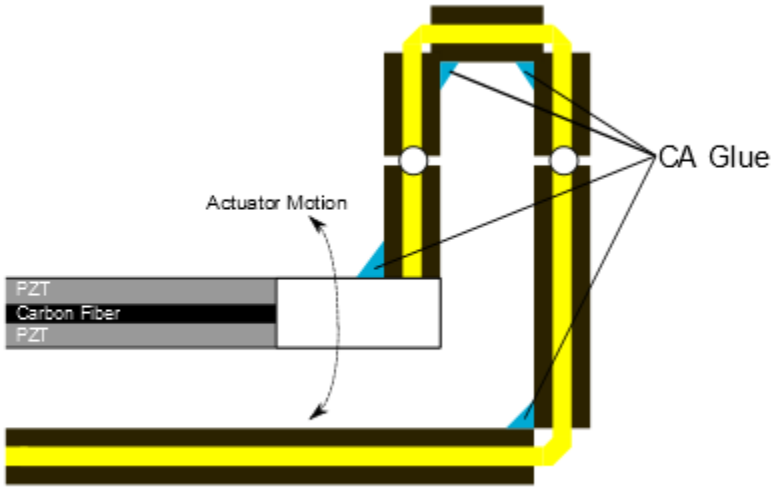

Figure 4.4: Side view of the folded transmission showing the relative position and motion of the actuator along with the different layers of the actuator

- Release Cuts: The resultant laminate post curing consists of an two carbon fiber layers each adhered to polyimide film by acrylic adhesive, with FR-4 at the top adhered to the upper carbon fiber layer. This cured laminate is then laser-machined with release cuts and release more features to facilitate folding.Top view of a cured laminated is shown in Fig.4.3

- Folding: The series of folds are performed under a microscope. A specially designed hinge is glued and folded into place manually.The transmission is folded and glued first in the series of folds, followed by rest of the airframe.

- Assembly: An actuator is carefully placed and glued down in the slots provided on the airframe. The actuator is also glued at the tip with the transmission. This is followed

by attaching a wing or tail to the transmission, the procedure finishes off one unit which looks like as shown in Fig.4.4.

- Soldering: Wire tethers are then soldered onto the actuators' bases to complete the electric connections.

Chapter 5

FEEDFORWARD CONTROLLER DESIGN

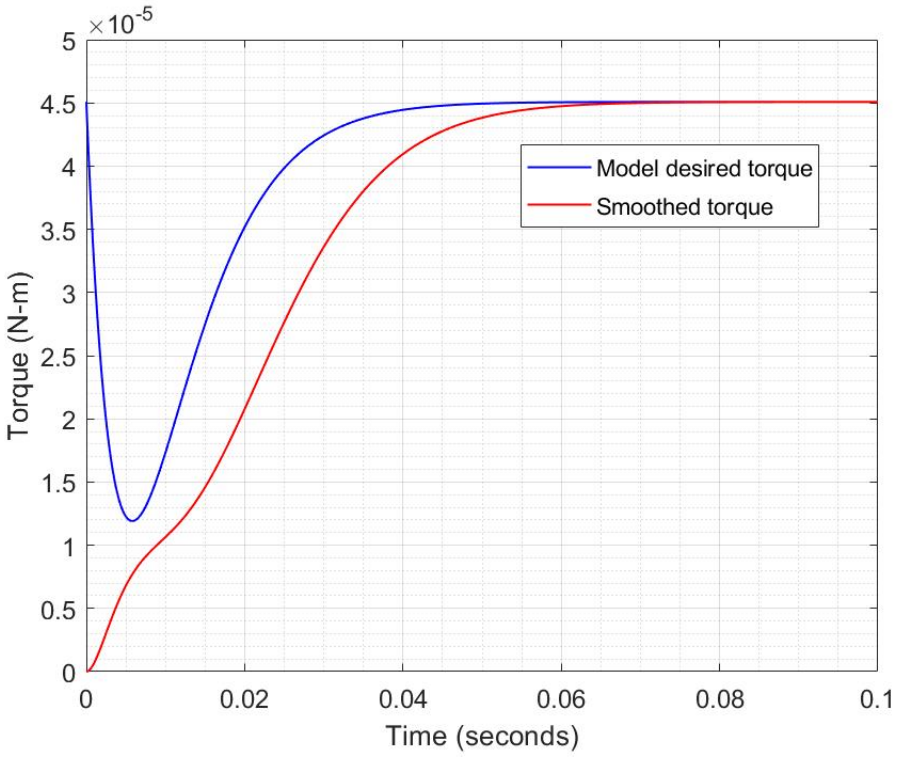

Figure 5.1: Torque predicted by the feedforward controller when emulating a critically damped reorientation (blue) and the torque after the smoother is applied to prevent the actuator from damage (red).

The robot's small size and payload limits currently preclude on-board sensing and feedback control of tail angle. Fortunately, the piezo actuator's spring-like mechanics greatly simplify control when compared to an idealized DC motor – quasistatically, the tail angle

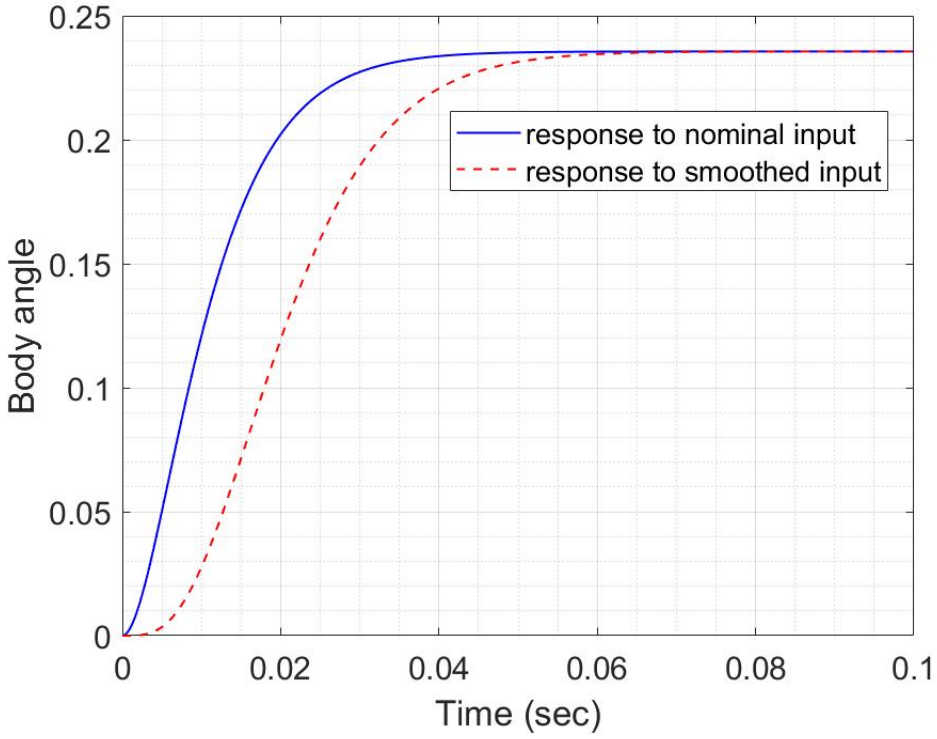

Figure 5.2: Simulated response to both nominal and smoothed signal. This indicates that neither excites the resonant mode in simulation.

can be controlled in open loop by modulating voltage (e.g. when $\tau_a = 0$ in Equation. 2.1). However, these same properties result in large, underdamped oscillations when the tail voltage is applied as a step (see Fig. 6.2), which would be transmitted to the body in equal proportion via Equation. 2.3.

To reduce these oscillations, we designed a time-varying open loop voltage waveform to replace the step input. Since the system dynamics are linear and second order, we designed a critically-damped trajectory based on a Proportional-derivative controller,

$$I_b\ddot{\theta}_b = \tau_b = K_P(\theta_{b,ref} - \theta_b) - K_D\dot{\theta}_b, \tag{5.1}$$

where τ_b is the total torque applied to the body, and for critical damping, $K_D = 2\zeta\sqrt{K_P I_b}$.

For a step in $\theta_{b,ref}$, the critically-damped response is,

$$\theta_b(t) = \theta_{b,ref}(1 - e^{-\sqrt{K_P/I_b}t} - te^{-\sqrt{K_P/I_b}t}). \tag{5.2}$$

Because the actuator dynamics feature mechanical proportional feedback (i.e. spring torque), we let the proportional component of the torque be determined by the natural dynamics; matching terms in Equation. 2.5, $K_P = K/\xi$. The time-varying voltage required to make the open-loop response track the critically-damped trajectory is,

$$V(t) = \frac{K_D}{\rho}\dot{\theta}_b(t) \tag{5.3}$$

Differentiating Equation. 5.2 and plugging into Equation. 5.3 yields the open-loop signal we designed, as plotted in Fig. 5.1.

This response demands an instantaneous step up to maximum voltage at $t = 0$; to satisfy the frequency-band limits on actuator safety, we further smoothed the input. The smoother is a third-order low-pass transfer function with a time constant $\tau_s = 0.005$ seconds, $S(s) = 1/(\tau_s s + 1)^2$, resulting in the final input voltage (Fig. 5.1, red).

Chapter 6

EXPERIMENTAL RESULTS

We performed two types of experiments: first, to identify the model parameters needed to generate the open-loop voltage input, and second, to evaluate the performance of the open-loop trajectory.

6.1 Estimation of Effectiveness and Body Inertia

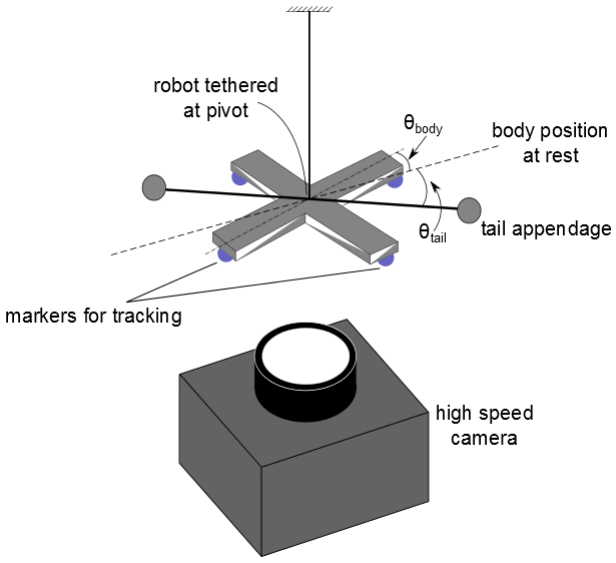

Figure 6.1: Diagram of apparatus used to estimate tail effectiveness on physical model of template dynamics. The robot is hung from its center of mass by a tiny Kevlar thread that allows it to rotate freely while its motions are recorded by high-speed camera.

To estimate the unknown model parameters, we conducted tethered experiments with

an open-loop linear ramped input to the wingless robot test platform. The template was tethered to a Kevlar fiber at its pivot with the tail free to actuate in the horizontal plane. The Kevlar fiber's torsional stiffness was negligible, and we added weights to counter any unbalanced gravitational forces and minimize pendular behavior. We excited the body-tail system with a ramp signal with a 0.1 s period and 150 V amplitude. Special markers are painted on the robot, and its motion was recorded using a high speed video camera (Sony RX-100). The video file was digitized using MATLAB and DLTv6 [40] and the discrete markers were tracked in each frame. This data can be used to measure the angles θ_b and θ_r.

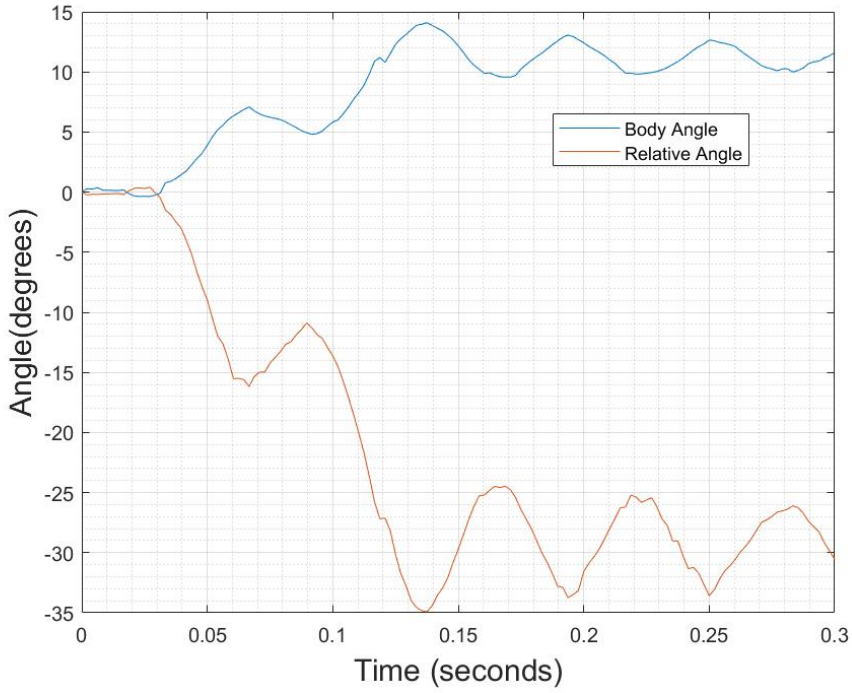

Figure 6.2: Time response of physical model of template dynamics to a ramp input. This data is used to estimate both tail effectiveness and spring stiffness.

Upon application of the ramp, the tail and body moved in opposite directions as expected (Fig.6.2). The motion featured large, underdamped oscillations of body and tail. We

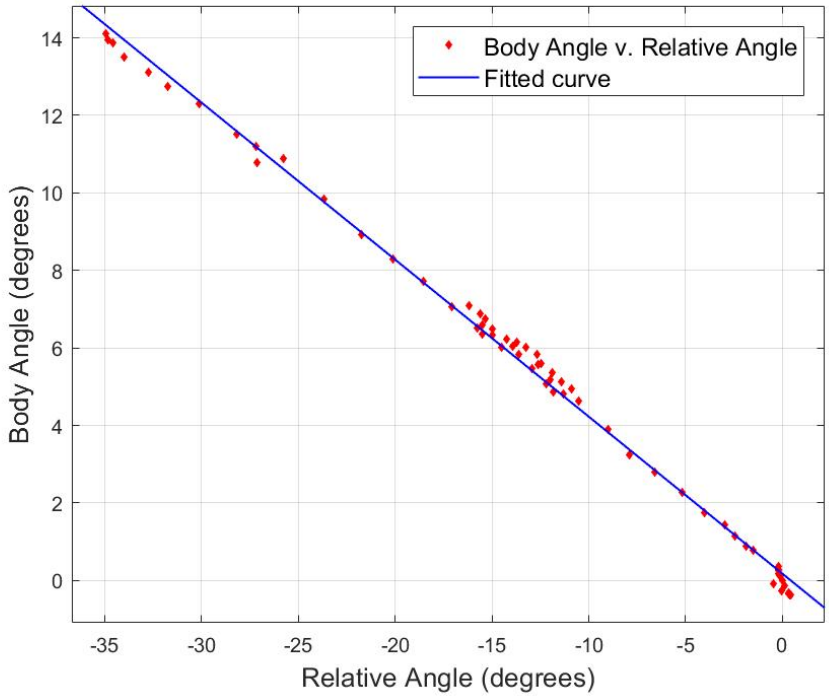

Figure 6.3: Measuring the tail effectiveness ξ. Body angle θ_b is regressed against tail angle θ_t as measured by high-speed camera.

estimated inertial effectiveness, ξ from kinematics using Eq. (2.3); ξ is the slope of the fit obtained from regressing θ_b on θ_r (Fig. 6.3). Our target effectiveness was $\xi = 0.5$; the actual measured value was approximately 18% lower due to our rough estimate of body inertia. We updated our estimate of body inertia using the tail inertia and Equation. (2.2) (assuming our tail inertia was more accurate, as it was generated by accurate measures of mass and length).

6.2 Measuring Actuator Characteristics

We estimated torsional stiffness, K, from the natural frequency of the oscillations following a step input to the tail with the body grounded. We estimated the period, T, of the oscillations

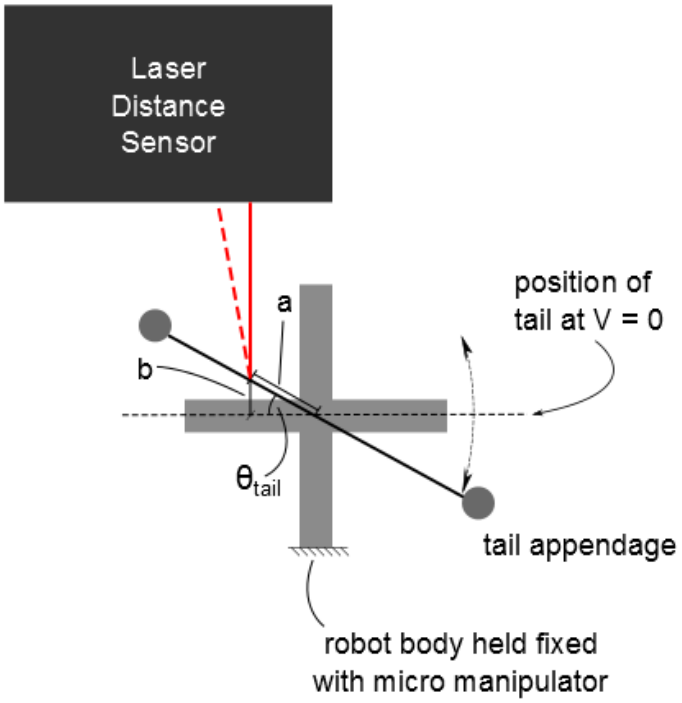

Figure 6.4: Method used to determine the torque voltage calibration ρ. The robot was held under a laser distance sensor measuring tail angle while the Voltage varied between ± 150.

and thus the damped natural frequency is $\omega_0 = \frac{2\pi}{T}$. Since it is an underdamped system with a very slowly-decaying resonance, its resonant frequency is very nearly equal to the undamped natural frequency ω_0, so, using the canonical relation $\omega_0 = \sqrt{K/I_t}$ we can rearrange to calculate $K = \omega_0^2 I_t$.

We identified the torque-voltage calibration, ρ, by observing the variation of angle as voltage increased. We held the robot fixed with a micro-manipulator under a laser distance sensor as shown in Fig 6.4. We measured distance to a known location on the appendage and used trigonometry to calculate the appendage angle. We varied input voltage between ± 150 V with the bias voltage kept fixed at 300 V. As expected, displacement was approximately linear with voltage (Fig. 6.5). We identified ρ from the slope using Equation. 2.1 with $\tau_a = 0$

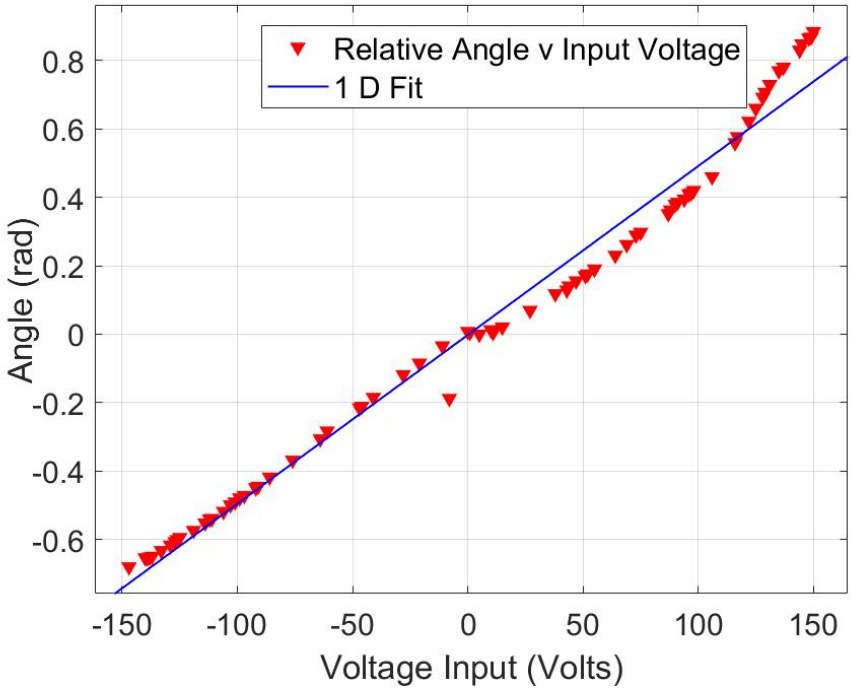

Figure 6.5: Appendage movement as a function of piezo voltage. The fit slope was used to estimate ρ.

(as the appendage was unloaded statically),

$$\theta_r = \frac{\rho}{K} V + \theta_{r0}, \tag{6.1}$$

where θ_{r0} is the rest angle of the appendage at zero voltage.

6.3 Reorientation behavior under feedforward control

Having identified the model parameters, we used the feedforward control in Equation. 5.1 to reorient the wingless robot in the tethered configuration. Compared to the ramp voltage trajectory (see Fig. 6.6), the control with emulated damping features a faster time to peak body rotation and a roughly 50% attenuation of oscillations post-reorientation. We attribute the remaining oscillation to imperfect estimate of the model parameters. Total reorientation

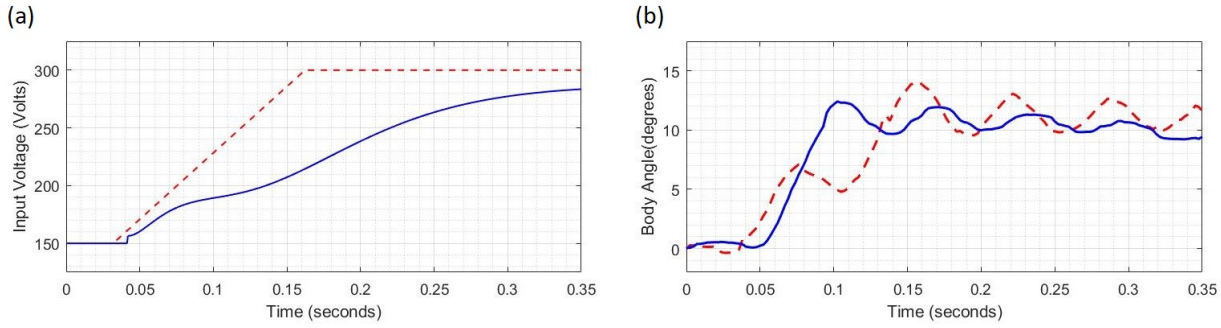

Figure 6.6: (a) shows the ramped unit step signal applied to the robot (dashed red) and open loop voltage output of the feedforward controller (blue) (b) shows response of the test robot to the ramped step input signal (dashed red) response of the test robot to the open loop voltage generated by the feedforward controller (solid blue). It is observed that the oscillations from open-loop voltage from the feedforward controller abate faster

was slightly under 15° with a half tail swing (the tail's rest position was halfway through the total stroke), corresponding closely with our 35° design spec. The slightly reduced body reorientation resulted from our initial underestimate of the body inertia and resulting lowered effectiveness.

6.4 Free Flight

Preliminary data taken from a free flight in which the robot flew briefly before actuating its tail is shown in Fig. 6.7. This system differed from the physical template system because of the need to minimize weight. Instead of a tail and body with coincident CM's, made possible through the addition of counterweights, the tail of this system extends only downward. Its length was 15 mm and mass was 20 mg, giving an effectiveness of approximately half of the physical template.

A visual inspection of the video shows that after takeoff but before tail actuation, the robot has initially rotated forward due to a small amount of applied pitch torque. After the

Figure 6.7: The robot initially rotates forward due applied pitch torque during tail actuation, after which it reverses direction, pitching backwards due to a shift in the system's CM. Each row shows frames from two separate flight videos

tail has actuated, the robot proceeds to reverse direction, pitching backwards. This indicates that the shift in the position of the CM resulting from the tail actuation results in a net torque acting on the body, $r \times f$, where "r" is the postition vector of the tail mass with respect to the CM of the robot and $f = m_t g$ is the gravitational force due to tail mass m_t.

Table 6.1: Design Parameters of Tail Template Insect Scale Robot

Parameter	Value	Units
ρ	0.4601×10^{-6}	$\mathrm{N\,m\,V^{-1}}$
ξ	0.406	(dimensionless)
K	95.87×10^{-6}	$\mathrm{N\,m\,rad^{-1}}$
I_b	15.01×10^{-9}	$\mathrm{kg\,m^2}$
m_t	22.8×10^{-6}	kg
l_t	15×10^{-3}	m
I_t	10.26×10^{-9}	$\mathrm{kg\,m^2}$

Chapter 7

CONCLUSIONS AND FUTURE WORK

In this report we described the modeling, analysis, design, and fabrication of an insect-sized robot with a piezo-actuated tail. It therefore departs from previous work in tail actuation that has exclusively been concerned with actuation by DC motor. Our results indicate that a key challenge that arises from the new actuator is that the system exhibits a slowly decaying resonant oscillation mode. We therefore present means to design a feedforward controller to avoid exciting this resonant mode of the piezo-tail system arising from its natural elasticity. To validate our analysis, we fabricated a physical system designed to replicate the simplest possible system that can produce net zero momentum Inertial Reorientation (IR) (Figs. 2.2 and 2.5). Our results show that the feedforward controller successfully reduces these oscillations. Furthermore, we showed tail actuation operating in flight to impart both a rotation and a torque on a freely-flying insect-sized aerial robot.

Our results provide a recipe for sizing the tail and feedforward controller for an arbitrary tail-actuated robot with any piezo-like springy actuator with unknown stiffness. It is as follows:

1. choose an effectiveness number for your tail so that it will be able to drive a desired body rotation magnitude $\Delta\theta_b$ given its maximum achievable tail rotation ($\sim 70°$for our system) according to $\xi = \Delta\theta_b/\Delta\theta_r$.

2. using a very rough estimate $\tilde{I}_b$ of your robot's moment of inertia, calculate the necessary tail inertia according to Eq. 2.2 as $I_t = \frac{\xi}{1-\xi}\tilde{I}_b$.

3. choose the maximum feasible tail length l_t (to minimize mass) and add a mass at its end according to $m_t = I_t/l_t^2$.

4. hang the robot-tail system from its center of mass by a thin thread such as Kevlar so that it rotates freely.

5. excite the system with a ramp and measure the angle versus time of the body and tail using a computer vision system such as marker-based motion capture.

6. estimate the true effectiveness ξ of your tail by regressing θ_b against θ_t (Section 6.1). You may need to redesign your tail if the measured effectiveness is not as desired.

7. estimate the frequency ω_0 of the tail-body system by measuring the period of oscillations, from which you can calculate $K = \omega_0^2 / I_t$ (Chapter 5).

8. estimate ρ by applying a range of voltages V and regressing against θ_r (Chapter 6.2).

9. compute feedforward command according to chapter 5.

10. smooth the resulting signal to remove sharp peaks that could excite the actuator's self-resoant frequency by applying a third-order low-pass filter using MATLAB's `lsim` command.

11. scale and offset this command as necessary to perform actuations of different magnitudes (the system is linear and therefore its response invariant to these changes).

7.1 Future Work

This work forms the foundation for future small, piezo-actuated robots that must perform fast, dynamic maneuvers such as fast midair turns or precise pose alterations before landing. Future work will attempt to identify how to find mass and speed-optimal piezo and tail configurations, as was performed for DC motors in [19].
Other Future work tasks include:

- Identification of the dynamics for the flying system

- Examine role of factors affecting transmission stiffness and actuator stiffness Examine role of factors affecting transmission stiffness and actuator stiffness

- Robot performing unsteady maneuvers such as controlled landing with the tail alone and rapid reorientation to avoid obstacles.

BIBLIOGRAPHY

[1] J. P. Whitney, P. S. Sreetharan, K. Y. Ma, and R. J. Wood, "Pop-up book mems," *Journal of Micromechanics and Microengineering*, vol. 21, no. 11, p. 115021, 2011.

[2] J. B. Gafford, S. B. Kesner, R. J. Wood, and C. J. Walsh, "Microsurgical devices by pop-up book mems," in *ASME 2013 International Design Engineering Technical Conferences and Computers and Information in Engineering Conference*, pp. V06AT07A011–V06AT07A011, American Society of Mechanical Engineers, 2013.

[3] K. Y. Ma, S. M. Felton, and R. J. Wood, "Design, fabrication, and modeling of the split actuator microrobotic bee," in *Intelligent Robots and Systems (IROS), 2012 IEEE/RSJ International Conference on*, pp. 1133–1140, IEEE, 2012.

[4] A. M. Hoover and R. S. Fearing, "Fast scale prototyping for folded millirobots," in *Robotics and Automation, 2008. ICRA 2008. IEEE International Conference on*, pp. 886–892, Ieee, 2008.

[5] R. J. Wood, "The first takeoff of a biologically inspired at-scale robotic insect," *IEEE transactions on robotics*, vol. 24, no. 2, pp. 341–347, 2008.

[6] Z. E. Teoh, S. B. Fuller, P. Chirarattananon, N. Prez-Arancibia, J. D. Greenberg, and R. J. Wood, "A hovering flapping-wing microrobot with altitude control and passive upright stability," in *Intelligent Robots and Systems (IROS), 2012 IEEE/RSJ International Conference on*, pp. 3209–3216, IEEE, 2012.

[7] K. Y. Ma, P. Chirarattananon, S. B. Fuller, and R. J. Wood, "Controlled flight of a biologically inspired, insect-scale robot," *Science*, vol. 340, no. 6132, pp. 603–607, 2013.

[8] P. Chirarattananon, K. Y. Ma, and R. J. Wood, "Adaptive control for takeoff, hovering, and landing of a robotic fly," in *Intelligent Robots and Systems (IROS), 2013 IEEE/RSJ International Conference on*, pp. 3808–3815, IEEE, 2013.

[9] S. B. Fuller, M. Karpelson, A. Censi, K. Y. Ma, and R. J. Wood, "Controlling free flight of a robotic fly using an onboard vision sensor inspired by insect ocelli," *Journal of The Royal Society Interface*, vol. 11, no. 97, p. 20140281, 2014.

[10] S. Balasubramanian, Y. Chukewad, and S. B. Fuller, "A low-weight on-board camera and a neural network to control an insect-scale aerial and ground robot," in *2018 8th IEEE International Conference on Biomedical Robotics and Biomechatronics (BioRob)*, (Submitted).

[11] S. B. Fuller, E. F. Helbling, P. Chirarattananon, and R. J. Wood, "Using a mems gyroscope to stabilize the attitude of a fly-sized hovering robot," in *IMAV 2014: International Micro Air Vehicle Conference and Competition 2014, Delft, The Netherlands, August 12-15, 2014*, Citeseer, 2014.

[12] S. B. Fuller, A. Sands, A. Haggerty, M. Karpelson, and R. J. Wood, "Estimating attitude and wind velocity using biomimetic sensors on a microrobotic bee," in *Robotics and Automation (ICRA), 2013 IEEE International Conference on*, pp. 1374–1380, IEEE, 2013.

[13] E. F. Helbling, S. B. Fuller, and R. J. Wood, "Pitch and yaw control of a robotic insect using an onboard magnetometer," in *Robotics and Automation (ICRA), 2014 IEEE International Conference on*, pp. 5516–5522, IEEE, 2014.

[14] M. Graule, P. Chirarattananon, S. Fuller, N. Jafferis, K. Ma, M. Spenko, R. Kornbluh, and R. Wood, "Perching and takeoff of a robotic insect on overhangs using switchable electrostatic adhesion," *Science*, vol. 352, no. 6288, pp. 978–982, 2016.

[15] P. Chirarattananon, K. Y. Ma, and R. J. Wood, "Fly on the wall," in *Biomedical Robotics and Biomechatronics (2014 5th IEEE RAS & EMBS International Conference on*, pp. 1001–1008, IEEE, 2014.

[16] P. Chirarattananon, K. Y. Ma, R. Cheng, and R. J. Wood, "Wind disturbance rejection for an insect-scale flapping-wing robot," in *Intelligent Robots and Systems (IROS), 2015 IEEE/RSJ International Conference on*, pp. 60–67, IEEE, 2015.

[17] S. Lupashin, A. Schöllig, M. Sherback, and R. D'Andrea, "A simple learning strategy for high-speed quadrocopter multi-flips," in *Robotics and Automation (ICRA), 2010 IEEE International Conference on*, pp. 1642–1648, IEEE, 2010.

[18] T. Libby, A. M. Johnson, E. Chang-Siu, R. J. Full, and D. E. Koditschek, "Comparative design, scaling, and control of appendages for inertial reorientation," *IEEE Transactions on Robotics*, vol. 32, no. 6, pp. 1380–1398, 2016.

[19] T. Libby, T. Y. Moore, E. Chang-Siu, D. Li, D. J. Cohen, A. Jusufi, and R. J. Full, "Tail-assisted pitch control in lizards, robots and dinosaurs," *Nature*, vol. 481, no. 7380, p. 181, 2012.

[20] E. Chang-Siu, T. Libby, M. Tomizuka, and R. J. Full, "A lizard-inspired active tail enables rapid maneuvers and dynamic stabilization in a terrestrial robot," in *Intelligent Robots and Systems (IROS), 2011 IEEE/RSJ International Conference on*, pp. 1887–1894, IEEE, 2011.

[21] A. Jusufi, D. Kawano, T. Libby, and R. J. Full, "Righting and turning in mid-air using appendage inertia: reptile tails, analytical models and bio-inspired robots," *Bioinspiration & biomimetics*, vol. 5, no. 4, p. 045001, 2010.

[22] A. Jusufi, D. I. Goldman, S. Revzen, and R. J. Full, "Active tails enhance arboreal acrobatics in geckos," *Proceedings of the National Academy of Sciences*, vol. 105, no. 11, pp. 4215–4219, 2008.

[23] J. P. Dyhr, K. A. Morgansen, T. L. Daniel, and N. J. Cowan, "Flexible strategies for flight control: an active role for the abdomen," *Journal of Experimental Biology*, vol. 216, no. 9, pp. 1523–1536, 2013.

[24] J. P. Dyhr, N. J. Cowan, D. J. Colmenares, K. A. Morgansen, and T. L. Daniel, "Autostabilizing airframe articulation: Animal inspired air vehicle control," in *Decision and Control (CDC), 2012 IEEE 51st Annual Conference on*, pp. 3715–3720, IEEE, 2012.

[25] N. Kohut, D. Haldane, D. Zarrouk, and R. Fearing, "Effect of inertial tail on yaw rate of 45 gram legged robot," in *Adaptive Mobile Robotics*, pp. 157–164, World Scientific, 2012.

[26] C. Casarez, I. Penskiy, and S. Bergbreiter, "Using an inertial tail for rapid turns on a miniature legged robot," in *Robotics and Automation (ICRA), 2013 IEEE International Conference on*, pp. 5469–5474, IEEE, 2013.

[27] A. Patel and M. Braae, "Rapid turning at high-speed: Inspirations from the cheetah's tail," in *Intelligent Robots and Systems (IROS), 2013 IEEE/RSJ International Conference on*, pp. 5506–5511, IEEE, 2013.

[28] U. Saranli, M. Buehler, and D. E. Koditschek, "Rhex: A simple and highly mobile hexapod robot," *The International Journal of Robotics Research*, vol. 20, no. 7, pp. 616–631, 2001.

[29] G.-H. Liu, H.-Y. Lin, H.-Y. Lin, S.-T. Chen, and P.-C. Lin, "A bio-inspired hopping kangaroo robot with an active tail," *Journal of Bionic Engineering*, vol. 11, no. 4, pp. 541–555, 2014.

[30] R. Briggs, J. Lee, M. Haberland, and S. Kim, "Tails in biomimetic design: Analysis, simulation, and experiment," in *Intelligent Robots and Systems (IROS), 2012 IEEE/RSJ International Conference on*, pp. 1473–1480, IEEE, 2012.

[31] J. Zhao, T. Zhao, N. Xi, M. W. Mutka, and L. Xiao, "Msu tailbot: Controlling aerial maneuver of a miniature-tailed jumping robot," *IEEE/ASME Transactions on Mechatronics*, vol. 20, no. 6, pp. 2903–2914, 2015.

[32] A. Demir, M. M. Ankarali, J. Dyhr, K. Morgansen, T. Daniel, and N. Cowan, "Inertial redirection of thrust forces for flight stabilization," in *Adaptive Mobile Robotics*, pp. 239–246, World Scientific, 2012.

[33] R. J. Wood, B. Finio, M. Karpelson, K. Ma, N. O. Pérez-Arancibia, P. S. Sreetharan, H. Tanaka, and J. P. Whitney, "Progress on picoair vehicles," *The International Journal of Robotics Research*, vol. 31, no. 11, pp. 1292–1302, 2012.

[34] W. S. Trimmer, "Microrobots and micromechanical systems," *Sensors and actuators*, vol. 19, no. 3, pp. 267–287, 1989.

[35] B. M. Finio, N. O. Pérez-Arancibia, and R. J. Wood, "System identification and linear time-invariant modeling of an insect-sized flapping-wing micro air vehicle," in *Intelligent Robots and Systems (IROS), 2011 IEEE/RSJ International Conference on*, pp. 1107–1114, IEEE, 2011.

[36] R. Full and D. Koditschek, "Templates and anchors: neuromechanical hypotheses of legged locomotion on land," *Journal of Experimental Biology*, vol. 202, no. 23, pp. 3325–3332, 1999.

[37] Y. Chukewad, A. Singh, J. James, and S. B. Fuller, "A robot fly composed of actuator units folded from a single laminatesheet, capable of ground locomotion, takeoff and landing," in *Intelligent Robots and Systems (IROS), 2011 IEEE/RSJ International Conference on*, (Submitted).

[38] J. James, V. Iyer, Y. Chukewad, S. Gollakota, and S. B. Fuller, "Liftoff of a 190 mg laser-powered aerial vehicle: The lightest untethered robot to fly," in *Robotics and Automation, 2008. ICRA 2018. IEEE International Conference on*, Ieee, 2018.

[39] A. Singh, Y. Chukewad, and S. B. Fuller, "A robot fly design with a low center of gravity folded from a single laminate sheet," in *Workshop on Folding in Robotics, IEEE conference on Intelligent Robots and Systems*, 2017.

[40] T. L. Hedrick, "Software techniques for two-and three-dimensional kinematic measurements of biological and biomimetic systems," *Bioinspiration & biomimetics*, vol. 3, no. 3, p. 034001, 2008.